CHAPTER - 5

CORROSION INHIBITION PERFORMANCE OF FURYL, PYRIDYL SUBSTITUTED AZOLES AND PYRIMIDINES FOR MILD STEEL IN 1M H_2SO_4

5.1 INTRODUCTION

The corrosion and corrosion inhibition of iron in different environments have been reported in many research studies[1-5]. Azole and pyrimidine derivatives have been reported to be effective inhibitors against corrosion of metals in corrosive media[6]. The inhibition mechanism usually involves their interactions with the metallic surfaces through their adsorption sites where polar functional groups are regarded as reaction centres[7]. The inhibitor molecule bonded to the metal surface by chemisorption, physisorption or complexation with the polar groups acting as the reactive centres in the molecules[8]. A perusal of literature reveals that less work has been carried out on the study of the effect of ring size of heteroaromatic compounds for corrosion inhibition of mild steel in acid medium. In view of the above, an attempt was made to synthesize heteroaromatic five and six membered compounds by introducing –OH, -SH functionalities, furan and pyridine rings on the corrosion inhibition efficiency of pyrimidines and azoles. The presence of electron pairs on N/O, π-electron cloud of the aromatic five and six membered rings, aid the adsorption of the compounds on mild steel surface. Electrochemical and non-electrochemical techniques were used for the study. To substantiate the experimental results, theoretical calculations were computed by applying Density functional theory. The mild steel surface after treatment in the absence and presence of the inhibitors, were analysed by FTIR, SEM-EDS, XRD and AFM techniques. A probable inhibitive mechanism was proposed to explain the results. The amount of dissolved iron was estimated by atomic absorption spectroscopic method.

5.2 EXPERIMENTAL WORK

5.2.1 Synthesis of inhibitors: Synthesis of pyrimidine and azole derivatives[9]

(i) Synthesis of chalcones ($I_{a,b}$)

An ethanolic solution of acetophenone (0.01 mol) and furfural/2-pyridine carboxaldehyde (0.01 mol) in presence of catalytic amount of 40% KOH was stirred for

3 hours at room temperature. It was then poured over crushed ice and the product formed was recrystallized from ethanol.

(ii) Synthesis of pyrimidine derivatives (II_{a-d})

A mixture of chalcone (0.02 mol), thiourea/urea (0.02 mol) were dissolved in ethanolic sodium hydroxide and refluxed for 6 hours. The precipitate obtained was filtered, washed and recrystallized from ethanol.

(iii) Synthesis of azole derivatives (III_{a-d})

A mixture of chalcone (0.02 mol), hydrazine hydrate/hydroxylamine hydrochloride (0.02 mol) and glacial acetic acid (10 ml) in ethanol (25 ml) was refluxed for 6 hours. The mixture was concentrated by distilling out the solvent under reduced pressure and poured into ice water. The precipitate obtained was filtered, washed and recrystallized from ethanol. The reactions are presented in **Scheme 5.1 and 5.2**.

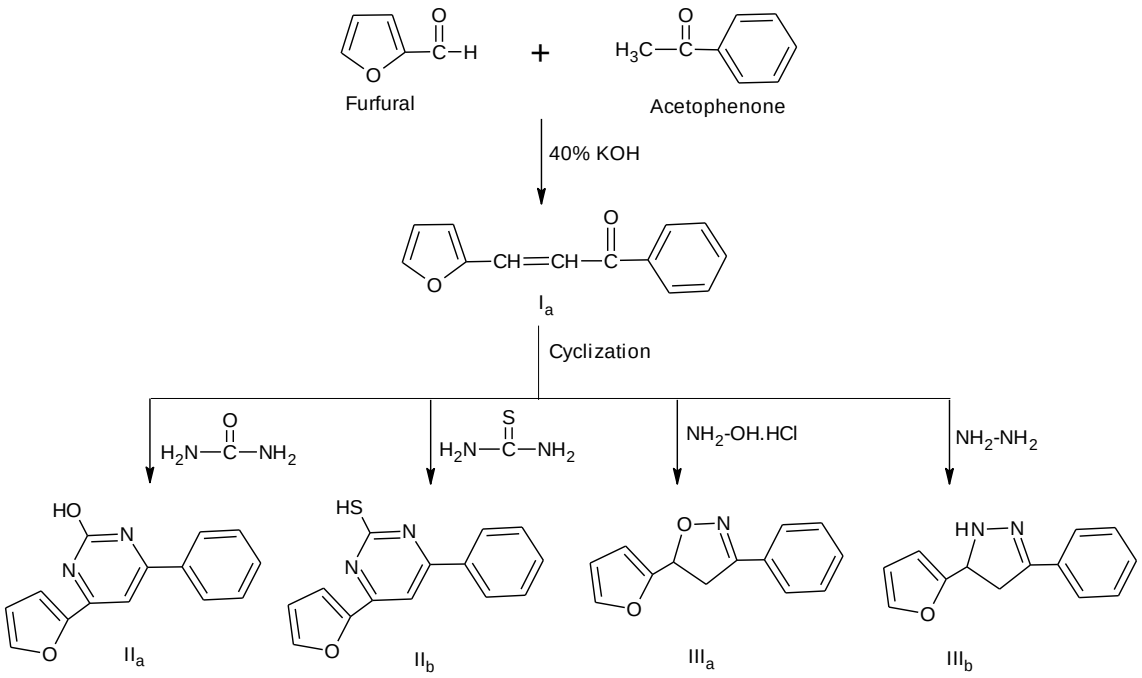

Scheme: 5.1

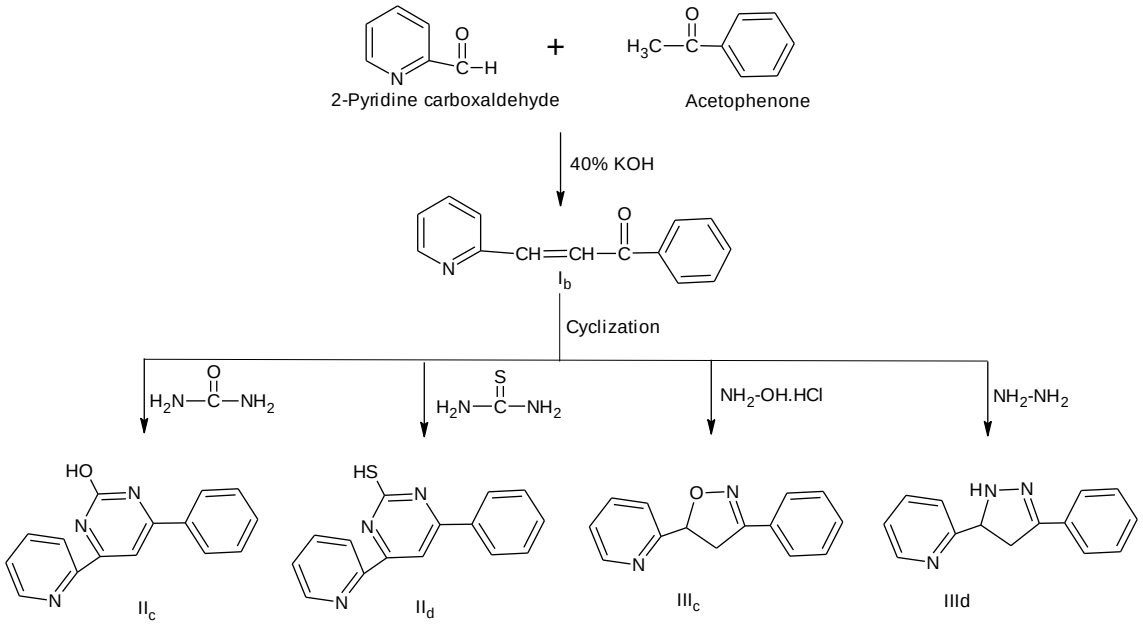

Scheme: 5.2

The synthesized compounds were characterized by FTIR spectra using IR Affinity 1 spectrometer (Shimadzu).

Code no.	Abbreviated name	Code no.	Abbreviated name
II_a	FPH	III_a	FPO
II_b	FPT	III_b	FPP
II_c	PPH	III_c	POP
II_d	PPT	III_d	PPP

5.2.2 Evaluation of inhibition efficiency of pyrimdine and azole derivatives

Non-electrochemical and electrochemical corrosion measurements were carried out, as reported in the previous chapters 3 and 4 of this thesis. 1M H_2SO_4 was prepared by dilution of analytical grade H_2SO_4 with distilled water. The concentration range of inhibitors used were 0.05 mM, 0.1 mM, 0.25 mM, 0.35 mM, 0.5 mM and 1 mM in 1M sulphuric acid. Surface morphology studies like FTIR, SEM-EDS, XRD and AFM were also carried out. Quantum chemical calculations were performed using Density functional theory method at B3LYP/6-31G(d,p) basis set.

5.3 RESULTS AND DISCUSSION

The inhibitors were synthesized by condensing acetophenone with furan/pyridine to get chalcones. The obtained chalcones were cyclized with urea/thiourea to get pyrimidine derivatives ($II_{a,b}$/$III_{a,b}$) with hydroxylamine hydrochloride/hydrazine hydrate to get azole derivatives. ($II_{c,d}$/$III_{c,d}$). The structure, colour, yield and melting point of the synthesized heterocyclic compounds are given in Table 5.1. The structure of the synthesized pyrimidines, oxazoles and pyrazoles were confirmed by IR spectra [4000 – 400 cm^{-1}] [Shimadzu IR affinity1]. The IR spectral data are presented in Table 5.2 (Figs. 5.1 - 5.8).

In pyrimidine derivatives bands characteristic of >C=N-, -OH, -SH, >C-O-C< stretching frequencies were observed around 1600 cm^{-1}, 3300 cm^{-1}, 2200 cm^{-1}, 1200 cm^{-1} respectively. Similarly for the pyrazoles and oxazoles bands characteristic of >C=N, -NH groups were observed around 1600 cm^{-1}, 3000 - 3100 cm^{-1} respectively.

5.3.1 Non-electrochemical methods

(i) Gravimetric measurements

Corrosion inhibition efficiency of the inhibitors (pyrimidines, azoles) calculated by weight loss measurements after 3 hours of immersion time at 303 K are listed in Table 5.3. The data in Table 5.3 reveal that inhibition efficiency increases with an increase in concentration of the inhibitor (0.05 mM – 1 mM). The increase in inhibition efficiency with increasing concentrations of inhibitors is due to an increase in the surface coverage, resulting in retardation of metal dissolution[10]. The anodic dissolution of iron in acidic and the corresponding cathodic reaction has been reported as follows[11]

$$Fe \longrightarrow Fe^{2+} + 2e^{-} \longrightarrow 5.1$$

$$2H^{+} + 2e^{-} \longrightarrow H_2 \longrightarrow 5.2$$

As a result of these reactions, including the high solubility of the corrosion products, the metal losses weight in the solution. The efficiency of the inhibitors follows the order: For pyrimidine derivatives, PPT > FPT > PPH > FPH. For azole derivatives, PPP > POP ≅ FPP > FPO. In general the order for both pyrimidines and azoles put together is PPT > FPT > PPH > FPH > PPP > POP ≅ FPP > FPO. Maximum efficiency of 98.69% was observed for PPT and a minimum of 89.85% for FPO. The corrosion rates were much

less in the presence of inhibitors[12] as compared to in the absence of inhibitors. The decrease in corrosion rate and high inhibition efficiency (%) of the inhibitors could be attributed to the adsorption of the entire inhibitor molecule on the mild steel surface resulting in the formation of a protective adsorption film, which separates it from the corrosive medium.

In the inhibited solution, the corrosive rate is indicative of the number of free corroding sites remaining after some sites have been effectively blocked by inhibitor adsorption[13]. The effectiveness of the inhibitors for corrosion protection is mainly due to the presence of hetero atoms (O, N and S) and aromatic rings.

(ii) Effect of temperature

Temperature plays an important role on the progress of the corrosion reactions of mild steel in 1M H_2SO_4 solutions. An increase in temperature increases the energy of the reactants to form an activated complex which dissociates to yield the corrosion products[14]. The effect of temperature on inhibition reaction is highly complex, as many changes may occur on the metal surface such as rapid etching, rupture, desorption of the inhibitor and decomposition or rearrangement of the inhibitor. Weight loss measurements were done in the temperature range 303 - 333 K in the absence and the presence of the synthesized inhibitors in 1M H_2SO_4 solution and the corrosion rates were calculated. Data in Table 5.4 reveals that as temperature increases, weight loss and corrosion rates also increases. At 303 K the percentage inhibiton efficiency of the inhibitors at 1 mM concentration ranged from 89% - 98%. At 333 K the percentage inhibition ranged from 75% - 95%. The value of inhibition efficiency decreased with rise in temperature suggesting physical adsorption mechanism. These results indicate that the adsorption of the investigated compounds shield the metal surface at room temperature, but deshield from the surface with rise in temperature[15].

i) Activation parameters for corrosion processes

Thermodynamic and activation parameters play an important role in understanding the inhibitive mechanism. The apparent activation energy (E_a) for dissolution of mild steel in 1M H_2SO_4 can be expressed by Arrrhenius equation.

$$\text{Log CR} = \frac{-E_a}{2.303RT} + \log A \longrightarrow 5.3$$

where CR is the corrosion rate, E_a is the apparent activation energy, R is the molar gas constant, T is the absolute temperature (K) and A is the pre-exponential factor. Fig. 5.9 represents the Arrhenius plot of log CR against 1/T for the corrosion process of mild steel in 1M H_2SO_4 solution in the presence and absence of pyrimidine and azole derivatives at a concentration of 1 mM. From Fig. 5.9, the slope of each individual line was determined, activation energy was calculated by using the slope value (E_a = slope × 2.303 × R) and the calculated value of E_a are summarized in Table 5.5.

It is evident from Table 5.5 that the values of E_a are higher for inhibited solutions as compared to the uninhibited solution, indicating desorption of the inhibitor molecule from metal surface at higher temperature[16].

The values of standard enthalpy of activation (ΔH^o) and standard entropy of activation (ΔS^o) was calculated using the Transition state equation,

$$CR = \frac{RT}{Nh}\exp\left(\frac{\Delta S^\circ}{R}\right)\exp\left(-\frac{\Delta H^o}{RT}\right) \longrightarrow 5.4$$

where CR is the corrosion rate, R is the molar gas constant, T is the absolute temperature, h is the Planck's constant, N is Avogadro's number, $\Delta H°$ and $\Delta S°$ are enthalpy and entropy of activation. A plot of log CR/T against 1000/T (Fig. 5.10) gave straight lines with slope ($-\Delta H°/2.303R$) and an intercept of [$\log(R/Nh) + (\Delta S^0/2.303R)$] from which the activation and thermodynamic parameters ($\Delta H°$ and $\Delta S°$) were calculated and listed in Table 5.5.

The positive sign of $\Delta H°$ reflects the endothermic nature of mild steel dissolution process. The values of $\Delta H°$ indicate that the corrosion reaction needs high energy to occur with an increase of inhibitor concentration. This means that the energy barrier of the corrosion reaction is large and the activated complex or transition state complex is formed at a slower rate.

The large negative value of $\Delta S°$ for uninhibited solution indicates that the formation of activated complex is the rate determinig step and it represents an association rather than a dissociation step, meaning that a decrease in disorder takes place during the course of the tranistion from reactant to the activated complex[17]. The values of $\Delta S°$ increased in the presence of the inhibitors, indicating that an increase in disorder takes

place during the course of the transition from reactant to the activated complex during the corrosion process.

(iv) Adsorption isotherm

Adsorption of an adsorbate on a metal-solution interface is considered as a substitutional adsorption process between the organic molecule in the aqueous solution, $Org_{(sol)}$ and the water molecules adsorbed on the metallic surface, $H_2O_{(ads)}$

$$Org_{(sol)} + xH_2O_{(ads)} \longleftrightarrow Org_{(ads)} + xH_2O_{(sol)}$$

where x is the size ratio representing the number of water molecules replaced by one molecule of organic adsorbate. The adsorption process reaches equilibrium when the chemical potential on the left side of the equation is equal to that of right. Depending on the means of expressing the chemical potential (site fractions, mole fractions *etc.*,) various adsorption isotherms can be derived to describe the adsorption process[18, 19].

Basic information on the interaction between the inhibitor molecules and the metal surface can be provided by the adsorption isotherm. The data from weight loss obtained by means of direct method (weight loss method) are more reliable than the indirect methods like Tafel polarization curves and electrochemical impedance spectroscopy. Therefore, the degree of surface coverage calculated from weight loss measurements corresponding to different concentration of heterocyclic inhibitors were used to study the adsorption behaviour of the heterocyclic inhibitors and to choose the more suitable adsorption isotherm. Attempts were made to fit the θ values to various isotherms including Temkin, Flory-Huggin and Langmuir are presented in Figs. 5.11 - 5.13 respectively. The correlation coefficient was used to choose the isotherm that best fits the experimental data in Tables 5.6 and 5.7. The Langmuir adsorption isotherm was found to be best to describe the adsorption behaviour of the synthesized inhibitors on mild steel. The Langmuir isotherm is based on the assumption that all adsorption sites are equivalent and that particle binding occurs independently from nearby sites, whether occupied or not [20]. According to this isotherm, θ is related to C by:

$$\frac{C_{(inh)}}{\theta} = \frac{1}{K_{ads}} + C_{(inh)} \longrightarrow 5.5$$

where K_{ads} is the equilibrium constant of the inhibitor adsorption-desorption process and $C_{(inh)}$ is the inhibitor concentration. Fig. 5.13 shows the plot of C/θ against inhibitor

concentration (C) at 303 K and the expected linear relationship is obtained for all inhibitors with excellent correlation coefficient (R^2) (Table 5.7), confirming the validity of this approach. The slope values for all the inhibitors were found to be close to unity, suggesting that adsorbed inhibitor molecules form a monolayer on the mild steel surface and there is no interaction among the adsorbed inhibitor molecules. From the intercept of the straight lines (Fig. 5.13), the values of K_{ads} were calculated. Large values of K_{ads} obtained for all the inhibitors suggest strong adsorption and hence better corrosion inhibition efficiency. Using K_{ads} values the values of ΔG^{o}_{ads} were calculated by using the following equation.

$$\Delta G^{\circ}_{ads} = -RT \ln (55.5\ K_{ads}) \longrightarrow 5.6$$

$$K = \frac{\theta}{C(1-\theta)} \longrightarrow 5.7$$

where θ is the degree of surface coverage on the metal surface, C is the concentration of inhibitor, R is the molar gas constant and T is temperature. The ΔG°_{ads} is lesser than -20 kJ mol^{-1} indicating that all the inhibitors are physically adsorbed on metal surface as seen in Table 5.7. The negative values of (ΔG°_{ads}) reflect the spontaneous adsorption of the studied heterocyclic derivatives (pyrimidines and azoles) on mild steel surface in 1M H_2SO_4 solution [21].

(v) Thermodynamic parameters

Thermodynamic parameters such as enthalpy of adsorption (ΔH°_{ads}) and entropy of adsorption (ΔS°_{ads}) can be deduced from integrated version of the Van't Hoff equation expressed by[22]

$$\ln K_{ads} = -\frac{\Delta H^{\circ}_{ads}}{RT} + \frac{\Delta S^{\circ}_{ads}}{T} + \ln \frac{1}{55.5} \longrightarrow 5.8$$

The plot between ln K_{ads} vs. 1000/T (Fig. 5.14) for heterocyclic inhibitors in 1M H_2SO_4 gives straight lines with slope ($-\Delta H^{\circ}_{ads}$ /2.303R) and intercept (ΔS°_{ads} /R + ln 1/55.5). Calculated values of ΔH°_{ads} and ΔS°_{ads} are presented in Table 5.8.

The enthalpy of adsorption was also deduced from the Gibbs Helmholtz equation[23]

$$\frac{\partial(\Delta G^{\circ}_{ads}/T)}{\partial T} = \frac{-\Delta H^{\circ}_{ads}}{T^2} \longrightarrow 5.9$$

This equation can be arranged to give

$$\frac{\Delta G^{\circ}_{ads}}{T} = \frac{\Delta H^{\circ}_{ads}}{T} + K \qquad \longrightarrow \quad 5.10$$

The plot of ΔG°_{ads} /T with 1/T gives a straight line with slope equal to ΔH°_{ads} (Fig. 5.15). It can be seen from the figure that ΔG°_{ads} /T decreased with 1/T in a linear fashion.

It is indisputable that an endothermic adsorption process (ΔH°_{ads} > 0) refers to chemisorption, whereas an exothermic adsorption process (ΔH°_{ads} < 0) may involve either physisorption or chemisorption or both of the processes occurring together[24]. In an exothermic process, the distinction between physisorption and chemisorption is based on the absolute value of ΔH°_{ads} . For a physisorption process, the enthalpy of adsorption is considered to be lower than -40 kJ mol^{-1}, while for chemisorption[25], it approaches -100 kJ mol^{-1}. In the present study, the calculated values of ΔH°_{ads} in 1M H_2SO_4 are from -24.92 to -31.16 kJ mol^{-1} (Table 5.8). On the basis of the results of this study, it is apparent that the mechanism of adsorption between the inhibitor and metal surface is essentially physisorption. The positive value of ΔS°_{ads} (Table 5.8) in 1M H_2SO_4 arises from the substitution process, which can be attributed to an increase in the solvent entropy and more positive water desorption entropy. The increase in disorder is also interpreted in terms of more water molecules being desorbed from the metal surface by the inhibitor molecules[26]. Therefore, the values of ΔH°_{ads} obtained by both methods are in good agreement

5.3.2 Atomic absorption spectrophotometric studies

The amount of iron dissolved in the presence of heterocyclic inhibitors when mild steel specimens were exposed to 1M H_2SO_4 were calculated and presented in Table 5.9. It has been found that the amount of dissolved iron in the corrodent solution decreases with increase in concentration of the inhibitors and there is good agreement between values of percentage inhibition efficiency calculated from weight loss and AAS techniques.

5.3.3 Electrochemical mesasurements

5.3.3.1 Electrochemical impedance spectroscopy (EIS) measurements

Electrochemical impedance spectroscopy analysis provide insight into the kinetics of electrode processes as well as the surface characteristics of the electrochemical system

of interest. Figs. 5.16 a-h show Nyquist plots for mild steel in 1M H_2SO_4 in the absence and presence of different concentrations of the heterocyclic derivatives at 303 K. Nyquist plots consist of one capacitive loop with one time constant. The charge transfer resistance values (R_{ct}) are calculated from the difference in impedance at lower and higher frequencies, as described elsewhere[27]. To obtain the double layer capacitance (C_{dl}) the frequency at which the imaginary part of the impedance is maximum, ($-Z_{i\ max}$) and C_{dl} values are calculated from the followingequation:

$$C_{dl} = \frac{1}{2\pi R_{ct} f(-Z_i max)} \longrightarrow 5.11$$

where $f(-Z_i\ \max)$ is the frequency at which the imaginary part of the impedance is maximum. R_{ct} and C_{dl} derived from the impedance measurements are shown as a function of inhibitor concentrations. The interpretation of Nyquist Figs. 5.16 a-h allows to determine the electrochemical parameters of the steel electrode and to acquire information about the corrosion process and mechanism. The impedance parameter such as charge transfer resistance (R_{ct}), double layer capacitance (C_{dl}) and inhibition efficiency (% IE) were calculated and are listed in Table 5.10, which showed that the inhibition efficiency increases by increasing the concentration of the studied inhibitors. By increasing the inhibitor concentration the R_{ct} values increase but C_{dl} values decrease. The increase in the R_{ct} values is attributed to the formation of an insulating protective film at the metal solution interface. The decrease in C_{dl} values suggest a decrease in the local dielectric constant and/or an increase in the thickness of the electrical double layer, confirming the formation of a protective layer at the metal surface by the inhibitors. This type of behaviour can be generalized and explained by the Helmholtz model given in the following equations

$$C_{dl} = \frac{\varepsilon\varepsilon_0 A}{d} \longrightarrow 5.12$$

where ε is the dielectric constant of the medium, ε_0 is the permittivity of the free space, A is the effective surface area of the electrode and d is the thickness of the protective double layer formed by the inhibitors.

Characterization of the adsorption and desorption of film formation on the metal electrode surface may be studied by determining its capacitance C_{dl}. The decrease in the C_{dl} value is due to the adsorption of the inhibitors on the steel surface[28]. The adsorption

of these inhibitors on mild steel surface can occur either directly on the basis of donor–acceptor interaction between the π-electrons (of the double bonds, phenyl rings and furan/pyridine ring) and the vacant d-orbitals of steel surface atoms or interaction of them with or already adsorbed sulphate ions as proposed[29, 30]. Adsorption might also occur in the cationic form with positively charged part of the molecule oriented towards negatively charged metal surface. This fact supports the observed decrease in C_{dl} values in the EIS measurement at the corrosion potential.

Figs. 5.16 a-h indicate that the impedance response of mild steel in uninhibited 1M H_2SO_4 has significantly changed after the addition of heterocyclic inhibitors in the corrosive system. The results described above can be interpreted in terms of equivalent circuit of the electrical double layer shown in Fig. i, which has been used previously to model the iron-acid interface[31].

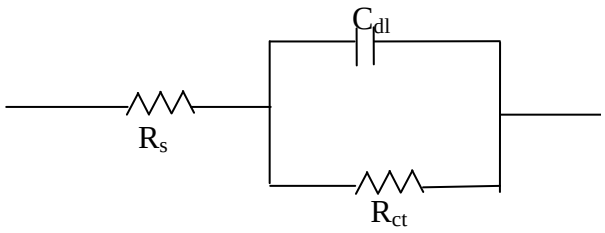

Fig. i: Equivalent circuit model for the studied system

Nyquist plots (Figs. 5.16 a-h) are depresssed and not perfect semi circles as a result of the roughness and other in homogeneities of the metal surface[32]. This kind of phenomena is known as ‘‘the dispersing effect’’. Also, it can be explained as follows: On the metal side, electrons control the charge distribution whereas on the solution side it is controlled by ions. Since ions are much larger than electrons, the equivalent ions to the charge on the metal will occupy quite large volume on the solution side of the double layer[31]. Decrease in the capacitance (C_{dl}) results from a decrease in dielectric constant and/or an increase in the thickness of the electrical double layer, suggesting that the inhibitor molecules act by adsorption at the steel-acid interface[33].

5.3.3.2 Potentiodynamic polarization measurements

Anodic and cathodic polarization curves for the corrosion of mild steel in 1M H_2SO_4 solution in the presence and absence of varying concentration of inhibitors at 303 K are shown in Figs. 5.17 a-h. The corrosion current density and corrosion potential

were calculated by extrapolation of linear parts of cathodic and anodic curves to the point of intersection. The electrochemical parameters such as corrosion potential (E_{corr}), corrosion current density (I_{corr}), anodic Tafel slope (b_a) and cathodic Tafel slope (b_c) and % IE determined from polarization curves are summarized in Table 5.11. The data in Table 5.11 clearly shows that the current density decreases in the presence of inhibitors which indicate that inhibitors are adsorbed on the metal surface and hence the inhibition efficiency increased with the increase in the inhibitor concentrations. It is apparent that from Figs. 5.17 a-h that the nature of the polarization curves remains same in the absence and presence of inhibitors, but the curves shifted towards the lower current density in the presence of inhibitors. The corrosion inhibition occurs due to blocking of the mild steel surface by adsorption of the inhibitor molecules through active centres. It is apparent from Table 5.11 that the values of b_a and b_c for all the studied inhibitors were found to change in the presence of inhibitors as compared to the values in the absence of the inhibitors (blank solution). Thus, the addition of the inhibitors in blank solution affected anodic dissolution of steel and cathodic evolution of hydrogen. The variation in the values of anodic and cathodic Tafel slopes in the presence of inhibitors suggests that the studied inhibitors are mixed type inhibitors[34]. However, the minor shift of E_{corr} values towards negative direction suggests the predominant cathodic control over the reaction.

5.3.4 Surface characterization

5.3.4.1 FTIR analysis of mild steel plate

The protective film formed over the mild steel surface by the inhibitor molecule was analyzed by FTIR spectroscopy. The FTIR spectra of adsorbed protective layer formed on the mild steel surface after immersion in 1M H_2SO_4 containing inhibitors (FPP and PPT) are shown in Figs. 5.18 and 5.19. From Fig. 5.18, it is revealed that >C=N stretching frequency at 1599.64 cm^{-1} shifted to 1620.17 cm^{-1} and >C-O-C< stretching frequency at 1220.99 shifted to 1216.17 cm^{-1} for the inhibitor (FPP). In PPT (Fig. 5.19), -SH stretching frequencies are shifted from 2063.92 to 2304.07 cm^{-1} and >C=N- shifted from 1589.41 to 1629.87 cm^{-1}. These progressive shifts in the wavelength of adsorption confirmed the protective film formed by the inhibitor molecules on the metal surface.

5.3.4.2 Scanning electron microscope-Energy dispersive X-Ray spectroscopy (SEM-EDS)

Scanning electron microscopy (SEM) is a wonderful technique used to examine the surface features with better understanding. In the present work, the SEM micrographs of mild steel in 1M H_2SO_4 solution in the absence and presence of inhibitor (PPT and FPT) after 3 hours exposure are shown in Figs. 5.20 - 5.22.

The SEM image in Fig. 5.20 shows the badly damaged surface of mild steel obtained after immersion in 1M H_2SO_4 for 3 hours without inhibitors. However, in the presence of inhibitors (PPT and FPT), the surface has remarkably improved with respect to its smoothness, indicating considerable reduction of corrosion as shown in Figs. 5.21 - 5.22. This improvement in surface morphology is due to the formation of a protective film of inhibitor on the mild steel surface which is responsible for retardation of corrosion.

The EDS spectra were used to determine the elements present on the surface of mild steel in the uninhibited and inhibited 1M H_2SO_4. The EDS analysis of uninhibited mild steel plate indicates the presence of only Fe and oxygen confirming that passive film on the mild steel surface contained only Fe_2O_3 (Fig. 5.23). EDS spectra of FPT showed additional lines characteristic of N and S as shown in Fig. 5.24. In addition, the intensites of C and O signals are enhanced. The appearance of the N and S signal and this enhancement in the C and O signals confirmed the presence of pyrimidine molecules on the metal surface. From the EDS spectra, it is evident that the % of Fe peaks is considerably reduced in the presence of inhibitors (FPT) which may be attributed due to the overlying inhibitor film[35]. A comparable elemental distribution obtained from the spectrum is presented in Table 5.12.

5.3.4.3 X-ray diffraction patterns

The corrosion products formed on mild steel exposed to acid medium have been studied by X-ray diffraction method. The patterns obtained clearly reveal the presence of metal and metal oxide phases. In Fig. 5.25 (blank), the peaks at $2\theta = 29.8$, 35.3, and 64.5° can be assigned to oxides of iron. Thus, the surface of the metal immersed in 1M H_2SO_4 contains iron oxides, which are most probably Fe_3O_4 and FeOOH, are found to be very

low. In Fig. 5.26 (PPT), the peaks due to iron alone observed at 2θ = 45.5° and 82.3° are very high[36]. This confirms the protection of mild steel by PPT.

5.3.4.4 Atomic force microscopy

The surface morphology of the mild steel specimens was further studied by AFM before and after corrosion in the absence and presence of 1 mM PPT. The surface morphology (2D and 3D image) of the mild steel specimens in the absence and presence of the inhibitor (PPT) in 1M H_2SO_4 is shown in Figs. 5.27 (a) and (b). It is clearly seen from the Fig. 5.27 (b) that the mild steel specimen shows rough surface due to acid corrosion. The average roughness of mild steel specimen immersed in 1M H_2SO_4 was found to be 126.19 nm. However, in the presence of 1 mM PPT corrosion is retarded and the surface of the inhibited mild steel specimen gets smoothened and average roughness was reduced to 52.97 nm. The decrease in roughness is probably due to the formation of adsorbed protective film of PPT on the mild steel surface.

5.3.5 Quantum chemical studies

5.3.5.1 Quantum chemical study of non-protonated form of the studied inhibitors in aqueous phase

Quantum chemical calculations based on density functional theory (DFT) method were performed on heterocyclic azole and pyrimidine derivatives as corrosion inhibitors for mild steel in acid media to investigate the relationship between molecular structure of the inhibitors and the corresponding inhibition efficiencies (IE %). The relation between inhibition efficiency of heterocyclic derivatives (azoles and pyrimidines) and some important quantum chemical parameters like E_{HOMO}, E_{LUMO}, dipole moment and E_{LUMO} - E_{HOMO} (ΔE), hardness, softness, electronegativity and the fraction of electrons transferred *etc.*, were investigated. These theoretical parameters were calculated in non-protonated as well as in the protonated form of selected heterocyclic derivatives (azoles and pyrimidines) in the aqueous phase as shown in Tables 5.13 and 5.16 respectively. In non-protonated form, the calculated quantum chemical parameters E_{HOMO}, energy gap, softness and fraction of electrons transferred follow the order, For azole derivatives: PPP > FPP > FPO > POP; Pyrimidine derivatives: FPH > FPT > PPH.

The above order does not correlate with the experimentally determined inhibition efficiency of the inhibitors.

The optimized structures of inhibitors and their highest occupied (HOMO) and lowest unoccupied (LUMO) molecular orbitals of heterocyclic derivatives in non-protonated and protonated forms are shown in Table 5.15 and 5.18 repectively.

5.3.5.2 Quantum chemical study of protonated form of the studied inhibitors in aqueous phase

The structural and electronic properties of heterocyclic derivatives (azoles and pyrimidines) were analysed and the results show that there is a strong effect on the chemical properties, specifically in the electron donating capability to the metal. In protonated structures, an acceptable planarity is reached in contrast to the non-protonated form, suggesting that the protonated structure has a greater capability of corrosion inhibition compared to the non-protonated form. Furthermore, the theoretical results show that for heterocyclic derivatives more stable structures are obtained when the protonation occurs at nitrogen and oxygen atoms. The preferred sites of azole and pyrimidine derivatives for protonation are FPH, FPT (N2, O24), FPO (N1, O2), FPP (N2, O9), PPH (N2, N24), POP amd PPP (N1, N23).

The energy of the highest occupied molecular orbital (E_{HOMO}), energy band gap (ΔE), softness and fraction of electrons transferred (ΔN) are displayed in Table 5.16. The data shows that the azole and pyrimidine derivatives can be ordered as PPP > POP > FPP > FPO and FPT > PPH > FPH. Thus, high values of E_{HOMO} facilitate adsorption and hence the inhibiton efficiency is improved.

It is clear from Table 5.16 that the protonated form of PPP and FPT exhibits the lowest E_{LUMO}, making the protonated form the most likely form for the interaction of mild steel with PPP and FPT molecules. Low values of the energy gap (ΔE) will provide good inhibition efficiencies, because the excitation energy to remove an electron from the last occupied orbital will be low[37]. A molecule with a low energy gap is more polarizable and is generally associated with a high chemical reactivity, low kinetic stability and is termed soft molecule[38]. The adsorption of inhibitor on metallic surface occurs at the part of the molecule which has the greatest softness and lowest hardness[39]. Quantum chemical parameters are listed in Table 5.16 indicates that for azole derivatives PPP and for

pyrimidine derivatives FPT was found to be an efficient inhibitor in H_2SO_4 which corresponds to the experimental results.

5.3.5.3 Mulliken charge density distribution

The more negative the atomic charges of the adsorbed center, more easily the atom can donates its electrons to the unoccupied orbital of the surface of the metal atoms and more easily the electrostatic attraction between the surface and the studied molecules. The Mulliken charge distributions for non-protonated and protonated forms are presented in Tables 5.14 and 5.17 respectively. In both non-protonated and protonated forms, nitrogen and oxygen atoms have higher charge densities. From the molecular orbital density distribution, Tables 5.15 and 5.18, it can be recognized that, the electron density of the frontier orbital is proportioned over several atoms. With this kind of structure, it is difficult to form chemical bond with active centers, which proves the probability of the physical adsorption between the interaction sites.

5.3.6 Mechanism of corrosion inhibition

The weight loss and electrochemical experiments reveal that the corrosion of mild steel is retarded in the presence of different concentrations of the inhibitors. The pyrimidine and azole derivatives block the surface of mild steel through adsorption mechanism. These compounds can be adsorbed in a flat orientation through tridentate (azole) and tetradentate (pyrimidines) form. The surface coordination is through the nitrogen, oxygen and sulphur. The mode of adsorption depends on the affinity of the metal towards π-electron cloud of the ring system. Metals such as Cu and Fe that have a greater affinity towards aromatic moieties were found to adsorb benzene rings in a flat orientation.

The values of thermodynamic parameters indicated that the adsorption of the azoles/pyrimidines on mild steel surface involves physisorption. The inhibitors get adsorbed on the mild steel surface by donor-acceptor interactions between the π-electrons of the benzene rings/heterocyclic rings and vacant d-orbital of the iron atoms.

According to the polarization results, the adsorption of the inhibitors follows the mixed inhibition mechanism. The inhibitors may get protonated and these cationic forms may adsorb directly on the cathodic sites of the mild steel and reduces the hydrogen

evolution reaction. The specific adsorption of anions having smaller degree of hydration such as sulphate ions is expected to be more adsorbed, they create an excess negative charge towards the solution and favour more adsoption of the cations[40]. On the other hand, the inhibitors may adsorb on anodic sites of mild steel through π-electrons of the aromatic rings and lone pairs of electrons of heteroatoms and therby inhibit the anodic dissolution of mild steel. Hence by following the above mechanism, the inhibitors show mixed inhibition behaviour on mild steel surface in 1M H_2SO_4 solution.

5.3.6 Evaluation of inhibitors

The order of inhibition efficiency of the pyrimidines and azoles are as follows pyrimidine derivatives: PPT > FPT > PPH > FPH

For azole derivatives: PPP > POP ≅ FPP > FPO

The performance of pyrimidine derivatives mainly depends on the size and the number of active centers present in the heterocyclic compound. This is enhanced by introducing –SH and –OH functionalities in the heteroaromatic system. Based on the results of weight loss and electrochemical measurements, it is predicted that, PPT exhibits a maximum inhibition efficiency of 98.69% at maximum concentration of 1 mM. This may be due to the presence of electron donating substituent SH in the structure, which induces to increase the electron density on the N atom of the pyrimidine moiety, resulting in an effective adsorption process leading to the formation of an insoluble protective film. In addition, the presence of phenyl ring and aromatic nature of pyridine ring are also responsible for higher protection efficiency. FPT shows 97.28% which is slightly lower than PPT. This is because furan has less aromatic character than pyridine. When compared to PPT and FPT, the inhibitors PPH and FPH have slightly lesser inhibiton efficiency of 94.71 and 90.19%, which may be due to the formation of intramolecular hydrogen bond of OH group with N atom of the pyrimidine ring.

It is predictable from the molecular structure of the azole derivatives that PPP and FPP have highest inhibition efficiency of 91.99% and 90.82%. This is due to the presence of >C=N azole group and –NH group in pyrazole moiety which is attached to pyridine/furan and aromatic rings in the molecule which can donate electrons thus increasing the reactivity of the molecule on the steel surface, whereas in POP and FOP

only azole group is present in oxazole moiety, the absence of –NH group in POP and FOP has probably reduced the percentage inhibition efficiency.

In general, in the above two series of compounds, the inhibitors with pyridine substitution perform slightly better than inhibitors with furan substitution. This may be attributed to the difference in ring size and greater electronegativity of the 'N' atom of the pyridine ring, which enhances the electron density on the pyridine ring. This favours greater adsorption of the pyridine substituted inhibitors in comparison to furyl substituted inhibitors.

5.4 CONCLUSIONS

- The efficiency of the inhibitors for pyrimidines and azoles follow the order:

  For pyrimidine derivatives: PPT > FPT > PPH > FPH

  For azole derivatives: PPP > POP ≅ FPP > FPO

- The investigated pyrimidine and azole derivatives inhibit the corrosion of mild steel in 1M H_2SO_4 solution and inhibition efficiency was found to increase with increasing concentration.
- The values of inhibition efficiency decreased with rise in temperature confirming physical adsorption mechanism.
- The adsorption of the inhibitors found to obey Langmuir adsorption isotherm.
- The variation in the values of anodic and cathodic Tafel slopes and the minor shift of E_{corr} values towards negative direction confirms the predominant cathodic control over the reaction.
- Electrochemical impedance spectroscopy measurements show that the charge transfer resistance increases and double layer capacitance decreases in the presence of azole and pyrimidine derivatives suggested the adsorption of the inhibitor molecules on the surface of mild steel.
- Inhibition action of the synthesized azole and pyrimidine derivatives takes place through its adsorption on the metal surface, which is confirmed by FTIR, SEM, EDS, XRD and AFM.
- Computed quantum chemical properties such as E_{HOMO}, E_{LUMO}, energy gap (ΔE), hardness (η), softness (S), the fractions of electrons transferred (ΔN) were found in good correlation with experimentally determined inhibition efficiency in protonated form.

5.5 REFERENCES

1. N.A. Darwish, F. Hilbert, W.J. Loreny, H. Rooswag, Electrochim. Acta., **18** (1973) 421.
2. J.L. Rao, B. Ren, Z.F. Huang, P.G. Cao, R.A. Gu, Z.O. Tian, Electrochim. Acta., **48** (2003) 1263.
3. A. Veawab, P. Tontiwachwuthi Kul, S.D. Bhole, Ind. Eng. Chem. Res., **264** (1997) 36.
4. B. Lai, Y. Zhou, P. Yang, Ind. Eng. Chem. Res., **51** (2012) 7777.
5. A. Veawab, P. Tontiwachwuthikul, A. Chalcma, Ind. Eng. Chem. Res., **40** (2001) 4771.
6. M. Zerfaoni, H. Oudda, B. Hammouti, S. Kertit, M. Benkaddour, Prog. Org. Coat., **51** (2004) 134.
7. Z. Tao, S. Zhang, W. Li, B. Hou, Ind. Eng. Chem. Res., **49** (2010) 2593.
8. L. Lukovits, E. Kalman, F. Zucchi, Corros., **57** (2001) 3.
9. A.F. Abbas, A.A. Turki, A. Jameel Hameed, J. Mater. Environ. Sci., **3** (2012) 1071.
10. A.U. Ezeoke, O.G. Adeyemi, O.A. Akerele, N.O. Obi-Egbedi, Int. J. Electrochem. Sci., **7** (2012) 534.
11. A. Mohammed, K.K.F. Amin, Corros. Sci., **52** (2010) 1762.
12. S. Kumar, D. Sharma, P. Yadav, M. Yadav, Ind. Eng. Chem. Res., **52** (2013) 14019.
13. I.O. Arukalam, I.O. Madu, N.T. Ijomah, C.M. Ewulonu, G.N. Onyeagoro, J. Mater., **(2014)**, 1.
14. N.A. Negm, F.M. Ghuiba, S.M. Tawfik, Corros. Sci., **53** (2011) 3566.
15. A.S. Fouda, M.A. Elmorsi, T. Fayed, M. Elsaid, Res. J. Chem.Sci., 4 (2014) 62.
16. A. Singh, A. Kumar Singh, M.A. Quarishi, Open Electrochem. J., **2** (2010) 43.
17. S.V. Ramesh, V. Adhikari, Bull. Mater. Sci., **31** (2007) 699.
18. H.P. Dhar, B.E. Conway, K.M. Joshi, Electrochim.Acta., **18** (1973) 789.
19. B.G. Ateya, J. Electroanal. Chem., **76** (1977) 191.
20. R. Solmaz, G. Kardas, M. Culha, B. Yazici, M. Erbil, Electrochim. Acta., **53** (2008) 5941.
21. J. Shukla, K.S. Pitre, Corrosion Rev., **20** (2002) 217.
22. E.A. Noor, J. Appl. Electrochem., **39** (2009) 1465.

23. M.A. Amin, S.S. Abdul El Rehim, H.T.M. Abdel-Fatah, Corros. Sci., **51** (2009) 882.
24. H. Jafari, I. Danaee, H. Eskandari, M. Rashvand Avei, Ind. Eng. Chem. Res., **52** (2013) 6617.
25. A.M. Badiea, K.N. Mohana, Corros. Sci., **51** (2009) 2231.
26. F.M. Donahue, K. Nobe, J. Electrochem. Soc., **112** (1965) 886.
27. S.S. Abdel-Rehim, M.A.M. Ibrahim, K.F. Khaled, J. Appl. Electrochem., **29** (1999) 593.
28. I.L. Rosenfeld, Corrosion Inhibitors, McGraw-Hill, New York, (1981).
29. T. Murakawa, S. Nagaura, N. Hackerman, Corros. Sci., **7** (1967) 79.
30. N. Hackerman, E.S. Snavely, J.S. Payne, J. Electrochem. Soc., **113** (1966) 677.
31. H. Ashassi-Sorkhabi, B. Shaabani, D. Seifzadeh, Electrochim.Acta., **50** (2005) 3446.
32. K.F. Khaled, Appl. Surf. Sci., **230** (2004) 307.
33. E. McCafferty, N. Hackerman, J. Electrochem. Soc., **119** (1972) 146.
34. D. Jayaperumal, Mater. Chem. Phys., **119** (2010) 478.
35. A.S.Fouda, S.Rashwan, Y.K.Elghazy, Int. J. Adv. Res., **1** (2013) 568.
36. D. Gopi, El-Sayed M. Sherif, V. Manivannan, D. Rajeswari, M. Surendiran, S. Kavitha, Ind. Eng. Chem. Res., **53** (2014) 4286.
37. A. Popova, E. Sokolova, S. Raicheva, M. Christov, Corros. Sci., **45** (2003) 33.
38. G. Gece, Corros. Sci., **50** (2008) 2981.
39. A. Dwivedi, N. Misra, Der pharma. Chem. **2** (2010) 58.
40. H. Wang, X. Wang, H. Wang, L. Wang, A. Liu. J. Mol. Model., **13** (2007) 147.